An Overview of Nuclear Magnetic Resonance

Disusun oleh:
Philips Nicolas Gunawidjaja

FAKULTAS MATEMATIKA DAN ILMU PENGETAHUAN ALAM
UNIVERSITAS KATOLIK PARAHYANGAN
BANDUNG
2007

Abstract

There are a number of techniques available for investigating the structures of materials. One of the most powerful techniques capable of providing information both about the structure of materials and about the dynamics of process within those materials is Nuclear Magnetic Resonance (NMR) Spectroscopy. The purpose of this paper is to give an overview on some of the most important aspects of the background theory of NMR.

Content

1. Introduction

Nuclear Magnetic Resonance (NMR) Spectroscopy is a powerful technique capable of providing information both about the structure of materials and about the dynamics of processes occurring within those materials. Even though many people in Indonesia might have heard of the term NMR, not many have a clear idea of what it is and how it can be used. The focus of this paper is to introduce some of the most important aspects of the background theory of NMR to the physics community in Indonesia. This introduction is based on articles and books written by Andrew [1], Eckert [2], Fitzgerald and de Paul [3], Duer [4], MacKenzie and Smith [5] and Harris [6].

2. The NMR Hamiltonian

Any nuclei containing an odd number of either protons or neutrons, or both, possesses angular momentum, I, and consequently a magnetic moment μ:

$$\mu = \gamma \hbar I^{*} \qquad (1)$$

where γ is a gyromagnetic ratio of the nucleus. The quantisation laws for angular momentum states that any nucleus with nuclear spin-quantum number I has $2I+1$ states. In the presence of an externally applied magnetic field of magnitude B_0 these states become non-degenerate due to the Zeeman interaction,

$$H_z = -\,\boldsymbol{\mu}.\boldsymbol{B}_0 \qquad (2)$$

where B_0 is taken to be along the z-axis. This then results in discrete energy levels

$$E_m = -\,m\gamma\hbar B \qquad (3)$$

* Bold alphabet indicate vector

where B is the magnetic field experienced by the nuclei, consisting of the external field B_0 and internal components B_{int} (usually $<< B_0$), which arise from internal interactions of the nuclei with their surrounding environment, hence

$$\boldsymbol{B} = \boldsymbol{B}_0 + \boldsymbol{B}_{int} \qquad (4)$$

Figure 1. shows the effect of an externally applied magnetic to the energy states of a spin ½ nucleus.

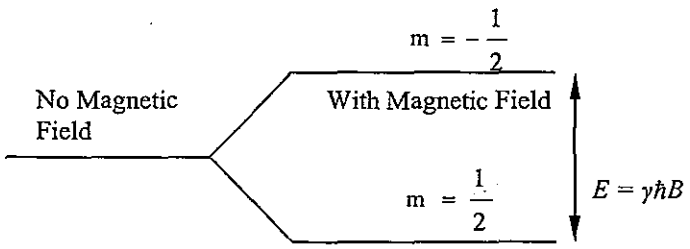

Figure 1. The effect of externally applied magnetic field on the energy of the m states of a spin ½ nucleus.

Since these internal fields are related to the structure of the material, their measurement is of central interest in NMR spectroscopy. To measure the energy differences between the magnetic spin states (and hence B_{int}), a second field, B_1, is applied in the direction perpendicular to B_0 (i.e. in the x-direction), whose amplitude oscillates at an angular frequency, ω_0, the frequency at which transitions between the energy states occur. At resonance the condition

$$\omega_0 = \gamma B \qquad (5)$$

holds. Where $\omega_0 = 2\pi\nu_0$, and ν_0, also known as 'Larmor frequency', is the frequency of the electromagnetic radiation at which absorption occurs. Typically for B = 1T, ν_0 = 42 MHz for protons.

The Fourier Transform (FT) of a rectangular pulse of duration τ_p applied at ν_0 is given by a sinc function with amplitude as a function of frequency:

$$A(\nu) = \frac{\sin \pi \tau_p (\nu_0 - \nu)}{\pi(\nu_0 - \nu)\tau_p} \qquad (6)$$

Therefore, from the bandwidth theorem, if a spectrum is to be acquired over $\sim 1/\tau_p$ Hz frequency range, the longest pulse length used should be $\sim \tau_p$ s. If a longer pulse were used, the amplitudes of any resonances far from the carrier frequency would begin to be attenuated by the sinc envelope given in equation 6, since they will not be excited to the same extent as resonances closer to the carrier frequency of the pulse. Figure 2. shows the Fourier Transform of a Radio Frequency (RF) radiation envelope created by 1 μs pulse.

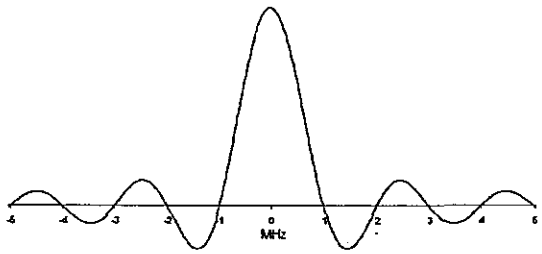

Figure 2. The RF radiation envelope created by a 1μs pulse. The x-axis is MHz from the carrier frequency of the pulse.

2.1. The Bloch Equations

The Bloch equations describe what happens to the precessing magnetisation immediately after the application of a 90° pulse. Bloch used a coordinate system that rotates around the *z*-axis in the *x*-*y* plane at the Larmor frequency. In this rotating frame, the decay of magnetisation can be written as:

$$\frac{dM_z}{dt} = \gamma(\mathbf{M} \times \mathbf{B})_z + \frac{M_0 - M_z}{T_1} \quad (7)$$

$$\frac{dM_x}{dt} = \gamma(\mathbf{M} \times \mathbf{B})_x - \frac{M_x}{T_2} \qquad (8)$$

$$\frac{dM_y}{dt} = \gamma(\mathbf{M} \times \mathbf{B})_y - \frac{M_y}{T_2} \qquad (9)$$

where T_1, in equation 7, refers to the longitudinal or spin-lattice relaxation time. T_2, in equation 8 and 9 is the transverse or spin-spin relaxation time. If the sample is placed in the B_0 field, initially it has no magnetisation, the magnetisation along the direction of the magnetic field then builds up as:

$$M_z(t) = M_0(1 - \exp(\frac{-t}{T_1})) \qquad (10)$$

After the application of a 90° pulse, the time taken for the magnetisation to completely relax back along the field is approximately $4T_1$. There are a number of mechanisms that can aid T_1 relaxation, which will be discussed briefly in section 6. For a sample with a short T_1, more acquisitions can be acquired in a given time period compare to a sample with a long T_1, so that higher signal to noise is accumulated in a given time. It is important to note that care needs to be taken with a sample with a range of T_1s. If the recycle time used is not $4T_1$ of the longest relaxing species, the shorter T_1 species will give a disproportionately larger signal than the long T_1 species, since the long T_1 species will have been partially saturated. Quantitative comparisons between two species cannot then be derived from spectra under conditions of partial saturation.

The component of magnetisation precessing in the *x-y* plane decays exponentially as the individual spins dephase, with relaxation time constant T_2:

$$M_x(t) = M_{x,t=0} \exp(\frac{-t}{T_2^*}) \qquad (11)$$

$$\frac{1}{T_2^*} = \frac{1}{T_2} + \frac{\gamma \Delta B}{2\pi}$$

Where T_2* is the effective T_2 relaxation responsible for the exponential decay envelope of the free induction decay of a Lorentzian line. There is a contribution from the inherent-decay processes and one from magnetic field inhomogeneity ΔB.

3. Internal Interaction Mechanisms

In general, the internal interactions B_{int} arise from the composite effect of a number of physically distinct interaction mechanisms. The three most important interactions in diamagnetic materials are magnetic dipole-dipole coupling (H_D), chemical shielding (H_{CS}), and for nuclei with spin quantum number >1/2, nuclear electric quadrupole coupling (H_Q). Therefore, the complete NMR Hamiltonian can be expressed as:

$$H = H_Z + H_D + H_{CS} + H_Q \quad (12)$$

The effects of H_{CS}, H_D, (and sometimes H_Q) upon the Zeeman energy levels are assumed to be minor compared to that of H_Z (termed the high field limit) and hence can be readily calculated by first-order perturbation theory. All of the above interactions are anisotropic. Consequently, the energy correction terms arising from the perturbation calculation contain an angular dependence, specifying the orientation of a molecular axis system relative to the applied magnetic field direction. In polycrystalline solids or glasses, the anisotropy of these internal fields in conjunction with their statistical orientation relative to B_0, give rise to a distribution of resonance frequencies. In the following sub-sections, the physical nature of these internal interactions will be discussed in more detail.

3.1. The Chemical Shift Interaction

The chemical shift interaction can be described as the effect of electron-nucleus interactions, which affect the local magnetic field experienced by the nuclei and hence influence their resonance frequencies. Four factors affecting the chemical shifts interactions consist of diamagnetic shielding by closed electronic shells, paramagnetic deshielding by

the angular momenta of admixed excited electronic states, shielding or deshielding effects from rapidly fluctuating paramagnetic electron spins, and shielding or deshielding effects due to conduction electrons at the Fermi level ("Knight shift"). Although these contributions are physically distinct, they are effectively not separable in an experiment. The chemical shift Hamiltonian, which is the most important in the materials studied here, can be written as:

$$\boldsymbol{H} = \mathbf{I}(1-\sigma)\mathbf{B}_0 \qquad (13)$$

where σ is an orientation-dependent tensor quantity termed the shielding.

In solution-state NMR spectroscopy, rapid molecular tumbling averages out this orientation dependence and produces a narrow line at a position known as the isotropic chemical shift (δ_{iso}), which reflects the average electronic environment of the nucleus (Figure 3a). In spectra of powdered solid samples, however, all orientations of a given site with respect to the B_0 field are present. When the local symmetry is less than cubic, most of these orientations have slightly different resonance frequencies. This leads to a broad lineshape known as a "powder pattern" from which the eigenvalues of the chemical-shielding tensor in its diagonal representation (σ_{11}, σ_{22}, σ_{33}) can be extracted (Figure 3.b,c). The chemical shielding (σ) which is the physical effect of the electrons is related to the chemical shift (δ) measured in the experiment by:

$$\delta = \frac{\sigma_{ref} - \sigma_{sample}}{1-\sigma_{ref}} \qquad (14)$$

The isotropic chemical shift is usually reported in units of parts per million (ppm):

$$\delta_{iso} = \frac{\nu_{iso} - \nu_{ref}}{\nu_{ref}} (\times 10^6) \qquad (15)$$

where ν_{ref} is the frequency of a suitable reference compound for the nucleus under investigation.

A useful consequence of this definition of the chemical shift is then the same ppm value will be measured for δ_{iso} regardless of the magnetic field employed. This also means that samples run at slightly different shim fields and in different probes can also be directly compared.

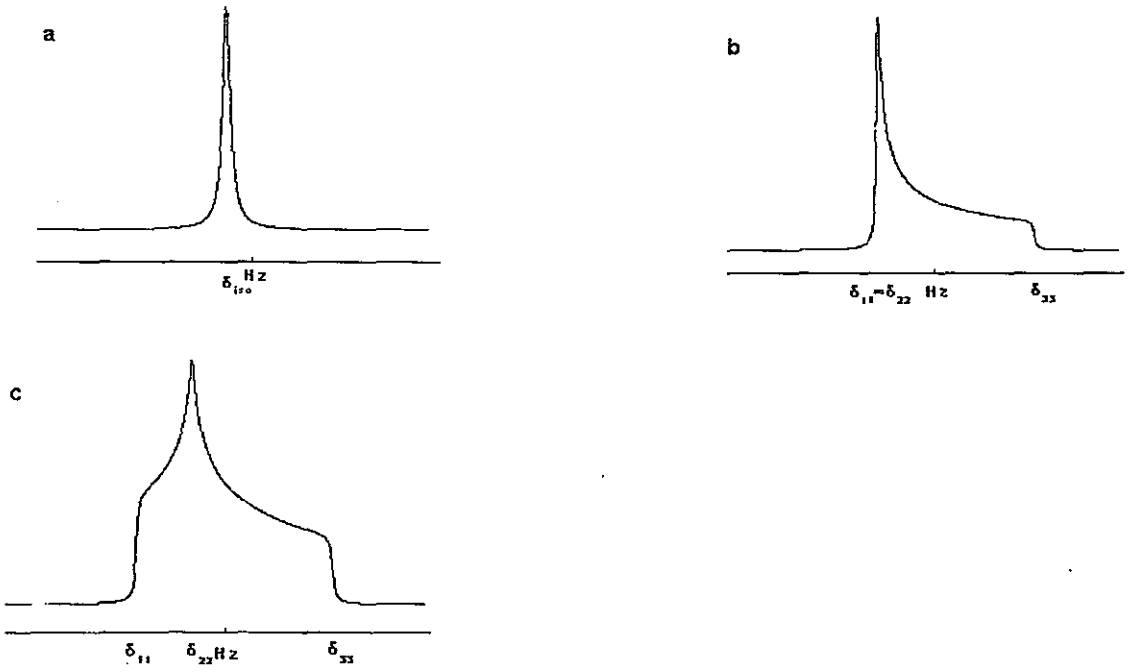

Figure 3. Typical chemical shift-dominated NMR powder patterns: (a) spherically symmetric, (b) axially symmetric, and (c) asymmetric chemical shift tensor [2].

The eigenvalues, which are referred to as the principal values of the chemical-shielding anisotropy (CSA), can be rewritten as [9]:

$$\delta_{iso} = \frac{1}{3}(\delta_{11} + \delta_{22} + \delta_{33})$$

$$\Omega = \delta_{11} - \delta_{33} \qquad (16)$$

$$\kappa = \frac{3(\delta_{22} - \delta_{iso})}{(\delta_{11} - \delta_{33})}$$

where $\delta_{11} \geq \delta_{22} \geq \delta_{33}$. In the above equation, the span, Ω defines the actual width of the powder pattern, while the skew, κ defines the asymmetry of the lineshape, similar to the

asymmetry parameter, η_{cs}, except that it varies from –1 to 1, removing the need to use a negative value of Ω to describe an oblate axial shift tensor.

3.2. The Dipole-Dipole Interaction

Another important interaction in solid state NMR is the magnetic dipole-dipole interaction which describes the effect of the local magnetic fields associated with the magnetic moments of surrounding nuclei. Two mechanistic contributions to this effect need to be considered: the "direct" (through-space) coupling and the "indirect" spin-spin coupling transmitted via polarisation of bonding electrons. For NMR spectra in solids, the first effect is usually dominant. The corresponding Hamiltonian describing the interaction between two spins with gyromagnetic ratios γ_1 and γ_2 separated by internuclear distance r is given by:

$$H_D = \frac{\mu_0}{4\pi} \cdot \frac{\gamma_1 \gamma_2 \hbar^2}{r^3} \{A + B + C + D + E + F\}^*$$

where $A = I_{1z} I_{2z} (3\cos^2\theta - 1)$

$$B = -\frac{1}{4}[I_{1+} I_{2-} + I_{1-} I_{2+}](3\cos^2\theta - 1)$$

$$C = -\frac{3}{2}[I_{1+} I_{2z} + I_{1z} I_{2+}](\sin\theta\cos\theta)\exp(-i\varphi)$$

$$D = -\frac{3}{2}[I_{1-} I_{2z} + I_{1z} I_{2-}](\sin\theta\cos\theta)\exp(+i\varphi)$$

$$E = -\frac{3}{4}[I_{1+} I_{2+}]\sin^2\theta\exp(-2i\varphi)$$

$$F = -\frac{3}{4}[I_{1-} I_{2-}]\sin^2\theta\exp(+2i\varphi) \qquad (17)$$

terms C to F are non-energy conserving and hence require energy exchange between the two spins and the rest of the system. This provides a means of T_1 relaxation, however during the timescale of an FID, these terms are negligible compared to the energy conserving terms A and B, therefore the Hamiltonian is often reduced by omitting terms C

* This equation is written in polar coordinates where $x = r\sin\theta\cos\varphi$, $y = r\sin\theta\sin\varphi$, and $z = r\cos\theta$

to F leaving only the secular terms A and B (provided the spins are the same). Term A is a classical interaction of the two magnetic moments and B is a *flip-flop* term describing the transition of the spins between spin-states. When the two spins coupling together are not of the same species, i.e. $\gamma_1 \neq \gamma_2$, the energy difference between spin states will be different for both species. Term B will no longer be energy conserving and in the secular approximation is again usually neglected. H_D is proportional to r^{-3}, therefore provided this is the dominant interaction it can be used to determine distance between nuclei.

As in the case of the chemical shift interaction, the direct dipolar interaction is anisotropic; it depends on the orientation of the internuclear vector with respect to the static B_0 field. Thus, for a powder sample, a broad lineshape will be generated. It is always axially symmetric as it is directed along the internuclear vector. This pattern can have a distinctive lineshape from which the dipolar coupling, and hence the internuclear distance can be calculated (Figure 4a,b)

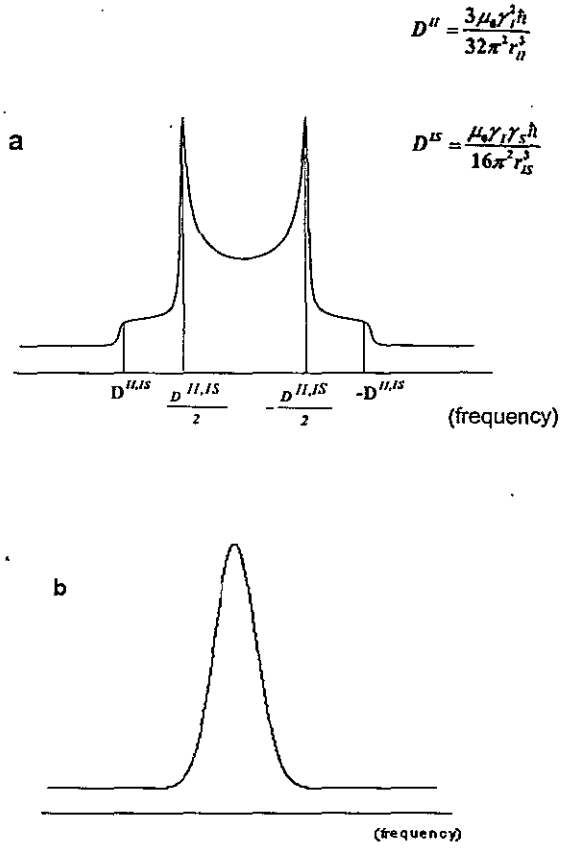

Figure 4. Typical powder patterns dominated by dipole-dipole couplings: (a) two mutually interacting spins (two-spin system), (b) many-spin system. [2,5].

3.2. The Nuclear Electric Quadrupole Interaction

The last perturbation of the nuclear magnetic energy levels which will be discussed, arises from the interaction of non-spherically symmetric nuclear electrical charge distributions ("nuclear electric quadrupole tensor") with the electric field gradient (EFG) generated by an asymmetric electrical charge distribution in molecules or at lattice sites. The Hamiltonian characterising this interaction can be written as:

$$H_Q = \frac{e^2qQ}{4I(2(I-1))}[3I_z^2 - I^2 + \eta(I_x^2 + I_y^2)] \qquad (18)$$

This interaction affects only nuclei with $I > ½$ in non-cubic environments. The anisotropy of the EFG is described by a traceless symmetric tensor, which can be diagonalised to give the components eq_{xx}, eq_{yy}, and eq_{zz} in a principal axis system. Since according to the Laplace equation:

$$\sum_i eq_{ii} = 0 \qquad (19)$$

only two principal components are independent. By convention, the quadrupolar interaction is then characterised by two parameters, e^2qQ/h and η. Where eQ is the scalar nuclear electric quadrupole moment, which expresses how much the nuclear electrical charge distribution deviates from spherical symmetry; $eq(=eq_{zz})$ is the major component of the electric field gradient, and η, defined as $(eq_{xx}-eq_{yy})/eq_{zz}$ $(0 \leq \eta \leq 1)$, characterises the deviation of the electric field gradient from cylindrical symmetry.

Depending on its strength compared the Zeeman interaction, the effect of the nuclear quadrupolar interaction on the solid state NMR spectrum can usually be calculated using either first- or second-order perturbation theory. Figure 5. shows an energy level diagram for a spin 5/2 nucleus. For half-integer spins, the central ½ to –½ transition is, to first-order, unaffected by the quadrupole interaction. In principle, e^2qQ/h $(=\chi_Q)$ and η can be evaluated from the shapes of the satellite transitions, which give rise to powder pattern similar to those shown in Figure 6. In many cases, however, these transitions extend over such a wide spectral region, that they often cannot experimentally be detected accurately.

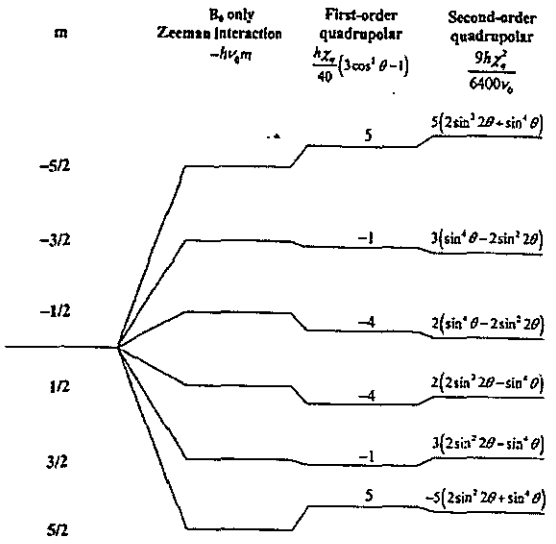

Figure 5. Energy level diagram for a spin 5/2 nucleus [5].

Stronger quadrupolar couplings necessitate treatment by second-order perturbation theory. To second-order, the lineshape of the central transition is then affected. The second-order energy correction is inversely proportional to the Larmor frequency, and exhibits a more complicated orientational dependence than the first-order effect. This is described by

$$\nu^{(2)}_{1/2,-1/2} = \frac{1}{16\nu_0}\left[\frac{3\chi_Q}{2I(2I-1)}\right]^2 [I(I+1)-3/4](1-\cos^2\theta)(9\cos^2\theta-1) \qquad (20)$$

Figure 7. shows the effect of the second-order quadrupolar interaction to the NMR lineshape. It can be seen that Magic Angle Spinning (MAS) reduces the linewidth by a factor of ~3-4 depending on η. The residual quadrupole interactions can produce distinctive lineshapes of the MAS centreband (Fig 7). The important point is that these effects scale with χ_Q^2 and inversely with ν_0. Hence results will change with magnetic field and when no quadrupolar lineshape can be observed the peak position is a function of magnetic field and can be used to estimate χ_Q.

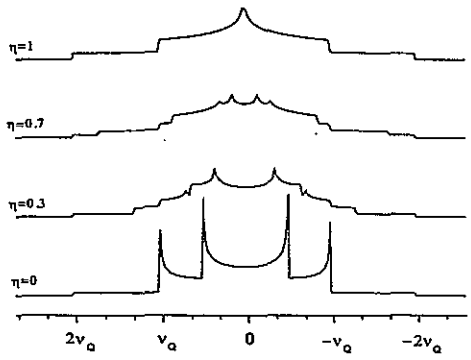

Figure 6. The quadrupole perturbed powder patterns for an I=3/2 nucleus showing the outer satellite transitions to first-order where $\nu_Q = (3\chi_Q)/(2I(2I-1))$.

4. Magic Angle Spinning

Magic angle spinning (MAS) is a technique, which allows high-resolution NMR spectra to be obtained from solid materials. This technique involves rotating the solid specimen about an axis inclined at the angle 54°44' to the direction of the magnetic field of the NMR magnet. This angle is $\cos^{-1}(1/\sqrt{3})$ and since several of the above interactions contain the term $(3\cos^2\theta - 1)$ where θ is the angle between the applied magnetic field and a direction which depends on the interaction. Sufficiently rapid rotation about this particular axis removes most broadening interactions from the NMR spectrum leaving only fine structure similar to the type which is found in NMR spectra of liquids. The narrowing results since these interactions to first-order transform as $(3\cos^2\beta - 1)(3\cos^2\theta - 1)$ under MAS. Hence although θ is different for each powder particle, they all pick up a common $(3\cos^2\beta - 1)$ dependence which can be set to zero.

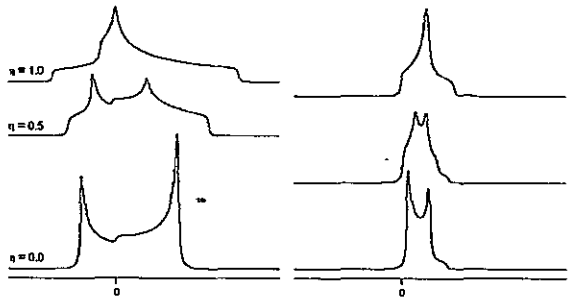

Figure 7. Simulated second-order quadrupolar central transition lineshapes. The x-axis is a frequency scale and is the same for both the static (left) and MAS (right) lineshapes [7]. No absolute units are put since the lineshapes scale with χ_Q^2/ν_0.

5. ^{13}C Cross Polarisation

While MAS leads to line narrowing and thus increases sensitivity as well as resolution, cross polarisation (CP) can be used to further enhance the sensitivity of a nucleus with a low gyromagnetic ratio [3, 8]. CP (Figure 8a) is a technique that is sensitive to heteronuclear dipolar coupling. This technique achieves magnetisation transfer from an abundant-spin system I (^{1}H) to the spin system of the observe-nucleus, S (^{13}C), whose signal is required. To accomplish this, the I-spins are first converted into a non-equilibrium state: a 90° preparation pulse followed by a strong B_1 field in phase with the transverse magnetisation which then forces the I-spins to stay parallel to the B_1 direction ("spin-locking"). In the spin-locking frame, immediately after the 90° pulse, the S-magnetisation is still M_s (parallel to z) with the same degree of order, but the energy levels are now much closer (i.e. $\gamma\hbar B_1$ as opposed to $\gamma\hbar B_0$). With the introduction of the field B_1, the system can now be assigned with an effective spin temperature T_{p1} defined by:

$$M_I = \frac{N_I\gamma_I^2\hbar^2 I(I+1)B_0}{T_L} = \frac{N_I\gamma_I^2\hbar^2 I(I+1)B_{II}}{T_{pI}} \qquad (21)$$

As $B_{II} << B_0$ and the degree of order amongst the spins remains the same (i.e. M_I is constant) it follows that:

$$T_{pl} = \frac{B_{1I} T_L}{B_0} \qquad (22)$$

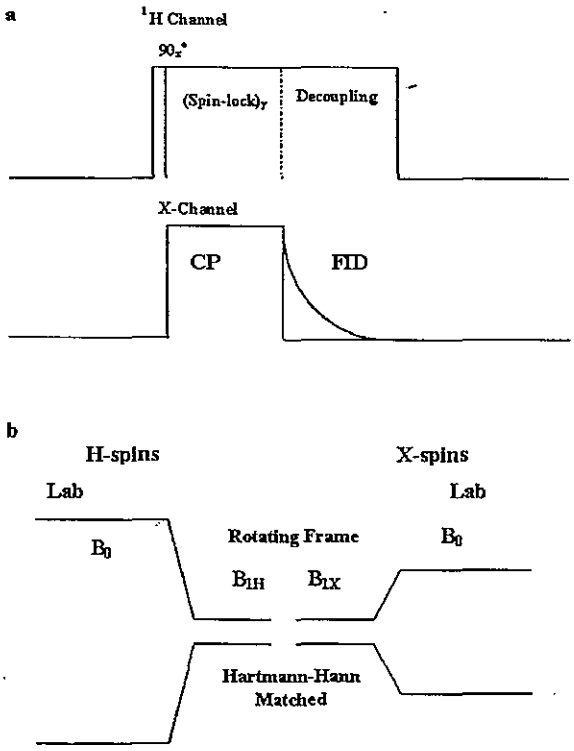

Figure 8. (a) Schematic representation of the CP sequence for $^1H \rightarrow X$. (b) The changes of the energy level from the laboratory frame and in the rotating frame showing the Hartmann-Hahn condition [5].

Hence the *I*-spins are effectively very cold. In contrast, the *S*-spins starts off with no transverse magnetisation, so in terms of thermodynamics, are very hot. There is a thermodynamic driving force for the transfer of magnetisation. However, the spin systems have to be allowed to communicate efficiently and this is achieved by applying a second B_1 field, this time to the *S*-spins. If the two spins to be brought in contact are spin ½ then the condition the two fields must meet is given by:

$$\gamma_I B_{1I} = \gamma_S B_{1S} \qquad (23)$$

This condition is known as the "Hartmann-Hahn condition" (figure 8b).

The rate of magnetisation transfer is characterised by the cross-relaxation time T_{cr}, which can be determined by variable contact time experiments. The stronger the dipole coupling, the shorter the cross-relaxation time.

6. Relaxation Mechanism

There are many mechanisms that contribute to T_1 and T_2 relaxation, however, only a simple model using thermal fluctuations will be presented here. T_1 and T_2 relaxation are caused by local fluctuations in the magnetic or electric field at the nucleus [10], and the change in local field from the average field B (δB) due to a thermal fluctuation can be written as

$$\delta \mathbf{B} = \mathbf{B} - \overline{\mathbf{B}} \tag{24}$$

where B is the actual field experienced by the nucleus and is $\overline{\mathrm{B}}$ the mean value. The relaxation times due to these field fluctuations can be described by the correlation time to over which the spin system is influenced by the fluctuation [11]:

$$\frac{1}{T_1} = \gamma^2(\overline{\delta B_x^2} + \overline{\delta B_y^2})\frac{\tau_0}{1+\omega_0^2\tau_0^2} \tag{25}$$

$$\frac{1}{T_2} = \gamma^2[\overline{\delta B_z^2}\tau_0 + \frac{1}{2}(\overline{\delta B_x^2} + \overline{\delta B_y^2})\frac{\tau_0}{1+\omega_0^2\tau_0^2}] \tag{26}$$

From the above result, at $\tau_o = 1/\omega_0$ the frequency of the fluctuations is the same as the Larmor frequency, and T_1 will be at a minimum. This is because the fluctuation that drives coherent transitions needs to have the same frequency as that corresponding to the transitions so that it can efficiently stimulate transitions between levels. The fluctuations also cause transverse T_2 relaxation through changing the phase of precessing spins to reduce the net precessing magnetisation. It is interesting to note that only the transverse x

and y components of the field fluctuations contribute to longitudinal T_1 relaxation, whilst both the longitudinal and transverse fluctuations of the field aid transverse T_2 relaxation.

T_1 relaxation can also be induced through the interaction mechanisms mentioned in section 1. Of these the quadrupolar interaction for a system with large χ_Q is potentially an efficient relaxation mechanism and can reduce T_1 to <0.5s, provided that fluctuations of the correct frequency are present.

The dipolar mechanism also aids T_1 relaxation, however, its effect is typically much smaller compared to quadrupolar and hyperfine interactions. For a spin-1/2 system which rely on the dipolar and thermal fluctuations for relaxation, T_1 times tend to be shorter for probe nuclei with higher dipole moments.

References

[1] E.R. Andrew, 'Magic Angle Spinning', *Encyclopedia of NMR*, Eds D.M. Grant and R.K. Harris (1996) 2891.

[2] H. Eckert, *Progress in NMR Spectroscopy*, **2** (1992) 159.

[3] J.J. Fitzgerald and S.M. de Paul, *Solid State NMR of Inorganic Materials*, Chapter 1, (1998) 19.

[4] M.J. Duer, *Solid State NMR, Principles and Applications*, Blackwell Science (2002).

[5] K.J.D. MacKenzie and M.E. Smith, *Multinuclear Solid State NMR of Inorganic Materials*, Pergamon (2002).

[6] R.K. Harris, *Nuclear Magnetic Resonance Spectroscopy*, Longman (1986).

[7] N. Dajda PhD Thesis, A Solid State Nuclear Magnetic Resonance Study of Industrial Inorganic Pigments, 2002, University of Warwick.

[8] S.R. Hartmann and E.L. Hahn, *Phys. Rev.*, **128** (1962) 2024.

[9] J. Mason Conventions for the reporting of nuclear magnetic shielding (or shift) tensors suggested by participants in the NATO ARW on NMR shielding constant at the University-of-Maryland, College-Park, July 1992, *Solid State Nuclear Magnetic Resonance*, **2** (1993) 285.

[10] A.P. Guimarães, *Magnetism and Magnetic Resonance in Solids*, John Wiley and Sons, New York, (1998).

[11] A. Carrington and A.D. McLachlan, *Introduction to Magnetic Resonance,* Harper, New York, (1998).